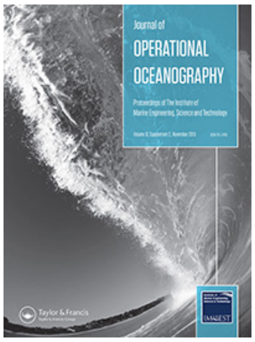

Taylor & Francis
Taylor & Francis Group

Journal of Operational Oceanography

ISSN: 1755-876X (Print) 1755-8778 (Online) Journal homepage: https://www.tandfonline.com/loi/tjoo20

Applications of ocean currents data from high-frequency radars and current profilers to search and rescue missions around Taiwan

Yung-Ting Shen, Jian-Wu Lai, Li-Guang Leu, Yi-Chieh Lu, Jau-Ming Chen, Huan-Jie Shao, Hsien-Wen Chen, Kuo-Tung Chang, Chuen-Teyr Terng, Yu-Chia Chang & Ruo-Shan Tseng

To cite this article: Yung-Ting Shen, Jian-Wu Lai, Li-Guang Leu, Yi-Chieh Lu, Jau-Ming Chen, Huan-Jie Shao, Hsien-Wen Chen, Kuo-Tung Chang, Chuen-Teyr Terng, Yu-Chia Chang & Ruo-Shan Tseng (2019) Applications of ocean currents data from high-frequency radars and current profilers to search and rescue missions around Taiwan, Journal of Operational Oceanography, 12:sup2, S126-S136, DOI: 10.1080/1755876X.2018.1541538

To link to this article: https://doi.org/10.1080/1755876X.2018.1541538

JOURNAL OF OPERATIONAL OCEANOGRAPHY
2019, VOL. 12, NO. S2, s126–s136
https://doi.org/10.1080/1755876X.2018.1541538

Applications of ocean currents data from high-frequency radars and current profilers to search and rescue missions around Taiwan

Yung-Ting Shen[a], Jian-Wu Lai[b], Li-Guang Leu[c], Yi-Chieh Lu[b], Jau-Ming Chen[d], Huan-Jie Shao[a], Hsien-Wen Chen[e], Kuo-Tung Chang[f], Chuen-Teyr Terng[g], Yu-Chia Chang[h] and Ruo-Shan Tseng[i]

[a]Department of Marine Biotechnology and Resources, National Sun Yat-sen University, Kaohsiung, Taiwan; [b]Taiwan Ocean Research Institute, National Applied Research Laboratories, Kaohsiung, Taiwan; [c]Department of Marine Science, ROC Naval Academy, Kaohsiung, Taiwan; [d]Department of Maritime Information and Technology, National Kaohsiung University of Science and Technology, Kaohsiung, Taiwan; [e]Department of Maritime Police, Central Police University, Taoyuan, Taiwan; [f]Department of Marine Environmental Engineering, National Kaohsiung University of Science and Technology, Kaohsiung, Taiwan; [g]Taiwan Central Weather Bureau, Taipei, Taiwan; [h]Department of Hydraulic and Ocean Engineering, National Cheng Kung University, Tainan, Taiwan; [i]Department of Oceanography, National Sun Yat-sen University, Kaohsiung, Taiwan

ABSTRACT
To enhance the immediacy and accuracy of search and rescue missions conducted by Taiwan Coast Guard Administration (TCGA), this study examines the characteristics of ocean currents and estimates the drifting trajectory of objects for two cases of marine incidents. Two methods are used to predict object's drift tracks: the first one is simply calculating the advection driven by currents and the second method adopts a Monte Carlo based software, SARMAP. Ocean currents data from a high-frequency radar system comprised of 18 radar units surrounding Taiwan supplemented by bottom-mounted Acoustic Doppler Current Profilers (ADCP) data and wind data are used as the primary oceanic environment data. The estimated ending points of drifting for both cases of missing persons in water by using both methods are consistent with the actual recovery locations. Our analyses demonstrate that ocean currents data, if properly used, can be very useful for rapid response in marine search and rescue.

ARTICLE HISTORY
Received 28 March 2018
Accepted 18 October 2018

KEYWORDS
Marine safety; search and rescue; high-frequency radar; ocean current; persons in water; wind leeway

1. Introduction

Each year numerous marine incidents occurred in the world oceans and at nearshore or coastal waters in many regions. These incidents result from a variety of causes, such as collisions, groundings, sinking of air/marine transportation vehicles, recreational and professional marine activities etc. A significant part of these incidents involves search and rescue (SAR) efforts organised by public personnel (i.e. Coast Guard, Navy) and/or private, voluntary helpers. An effective and timely SAR strategy would benefit various aspects of maritime security and safety, such as searching for missing persons in water (PIW) and saving lives at sea, finding lost objects like drifting vessels, containers, wrecks or debris, and reducing costs of search operations (Breivik et al. 2013).

Maritime SAR is essentially about determining the evolution of searching areas with time in as little time as possible from analysing a number of unknowns and factors such as the last known positions (LKP), the object's shape and the environmental forcing (wind, wave, and current), then rapidly deploy search and rescue units (SRU) in the search area. Among all factors, ocean current is the most important quantity which affects drifting trajectories of objects. Varying with different types and the immersion ratio of objects, wind forces acting on drifting object will induce leeway slip motion and divergent direction uncertainties. Ocean wave, although often considered to have minor effects on the fate of material floating on the surface, stands out as one of the most possible causes for the occurrence of marine incidents and also greatly influences the ensuing SAR operations (Zhang et al. 2017). There have been numerous accidents at sea related to the rough, stormy sea state or unexpected rogue waves, resulting in capsizing or sinking of ships. Therefore, the operational monitoring and prediction of wind, wave, and current are not only very important to the safety of marine transportation and navigation, but they also constitute essential elements for accurate prediction and effective marine SAR operations once accidents occur.

Accurate prediction for the fate of a drifting object and successful marine SAR operations depend strongly

CONTACT Ruo-Shan Tseng rstseng@mail.nsysu.edu.tw

on the accuracy of the forcing data (wind, waves and currents), particularly the ocean currents surface maps in real-time which are usually provided by high-resolution numerical models or high-frequency coastal radars. During the past several decades, high-frequency radar (HFR) has become a reliable and useful tool for mapping ocean surface currents with high resolutions in temporal and spatial scales since the pioneering study of Crombie (1955). The ability of HFRs to measure surface currents have been calibrated and validated through comparisons with surface velocities from satellite-tracked drifting buoys (Ohlmann et al. 2005, 2007) and point measurements from moored or shipboard ADCPs (Paduan et al. 2013). RMS differences of velocities between HFRs and in-situ measurements were reported to be between 10 and a few tens cm/s. In addition to surface currents, HFR can also provide some secondary products such as pointwise wave characteristics (wave height, wave period and direction), surface wind speed and direction. Because of the diverse and important applications, HFRs have seen a significant increase over the past two decades in the United States, Europe, Australia and Asia. For instance, a national network which is made up of more than 100 HFRs has been developed along the eastern and western coasts of the United States (Harlan et al. 2010). In the Mediterranean Sea, particularly in the Gulf of Naples, a growing number of HFR system has been deployed in the coastal areas (Falco et al. 2016).

Taiwan is an island surrounded by oceans with coastline over 1200-km long. Intensive recreational and professional activities in the coastal and offshore areas as well as busy marine transportation in combination with violent sea states during the prevailing winter northeastern monsoon and summer typhoon seasons in this region lead to many marine incidents. According to the Taiwan Coast Guard Administration (TCGA) statistics, there were approximately 5400 marine incidents reported during the period of 2003–2013 in the neighbouring waters. Each year there are on average 90 people missing or dead due to fishing boat accidents in Taiwan according to Fishery Agency statistics (Yao et al. 2016). Because of the large number of casualties and death as well as huge property losses due to marine incidents, the Taiwan Central Weather Bureau, Tourism Bureau, Water Resources Agency, Taiwan Ocean Research Institute, Harbor and Marine Technology Center, and TCGA have been working on building various ocean observing systems in an operational sense. For example, an HFR system which is composed of 18 radar units along the east and west coasts of Taiwan has been established and in routine operation since 2009. Details of this HFRs system will be presented in the next section. Another example is a marine monitoring network which is composed of 18 data buoys deployed in coastal waters and tens of bottom-mounted Acoustics Doppler Current Profilers (BM-ADCPs) at harbour entrances surrounding Taiwan has been established since 1997. This network measures marine meteorology and climate (i.e. wind, waves, current, and other variables) on a routine basis. One of the main applications of these observing system and network is for the marine safety.

In order to demonstrate the importance of ocean observing system to marine SAR, wind and current field data are used as oceanic environment input for two selected cases of marine incidents. The remaining of this paper is organised as follows: Section 2 introduces the HFRs system and two BM-ADCPs of Taiwan. Two simulation methods of object's drifting trajectory are described in Section 3, followed by the employment of these methods to two cases in Section 4. Discussions are presented in Section 5 and some concluding remarks are provided in Section 6.

2. Ocean observations

2.1. Operational high-frequency coastal radars

Taiwan Ocean Radar Observing System (TOROS) was initiated and established by the Taiwan Ocean Research Institute (TORI) in 2009. To date, this system is composed of 18 high-frequency radars (HFRs) units, made by CODAR, along the east and west coasts of Taiwan (locations are indicated by blue and green squares in Figure 1(a)). Figure 1(b) shows pictures of radar deployment and setup on the shore, including Rx and Tx antennas and control panels, for one station of DATN on the northwestern coast of Taiwan. Among the 18 HFRs, 12 of which are 5 MHz long-range type, 5 are 13 MHz medium range type, and 1 is 24 MHz standard range type (Table 1). The long-range model, for example, can provide an effective spatial observation radius up to 150–220 km with horizontal resolution around 3.75 km in the radial direction and 5° in azimuth. On the other hand, the range and bearing resolution of the 13/24 MHz system is 1.5 km and 2 degrees, respectively. In the radial combination of surface currents, the spatial grid resolution of the current is 10 km, and on each grid point, the radial velocities from different radar sites are searched for 15 km in search radius, and combined by CODAR SeaSonde software to produce hourly surface current map. Considering the uncertainty of radar observation and slow change of current, the so-called hourly flow field refers to the calculation of the radial velocity of the radar observation about 75 minutes before and after the moment. By means of overlapping systems, the coverage of surface

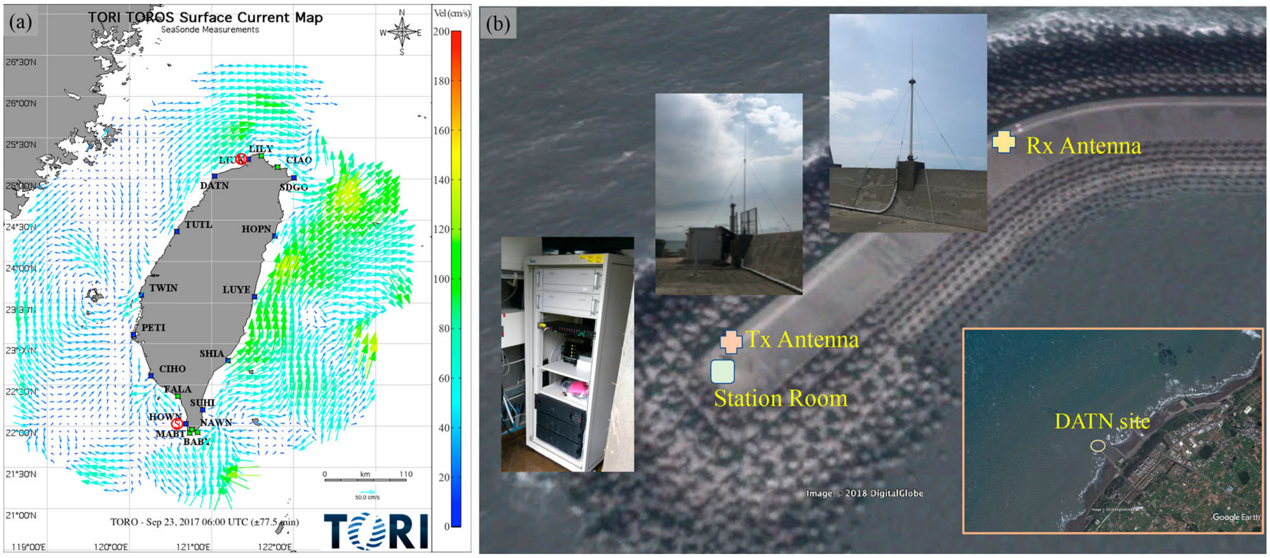

Figure 1. (a) Locations of long-range type (blue square) and standard type (green square) HF radar stations around Taiwan. Four-letter code denotes station name. Coloured vectors are a typical product of surface current field on 23 September 2017 in 10 km resolution. Two bottom-mounted ADCPs are located at 20-m depth off southwestern Taiwan (marked as S) and off northwestern Taiwan (marked as N). (b) Typical HFR setup on the shore. Photos show the antenna and control panels of one station DATN which is located on the northwestern coast of Taiwan.

current monitoring surrounding Taiwan is almost complete with the mapping area about 5.4 times the size of Taiwan. Starting from June 2016, an extra, temporary HFR station was setup on Fang-Liao (location FALA is marked in Figure 1(a)) to enhance coverage area and improve horizontal resolution off southwestern Taiwan. Combining FALA with the existing HFRs, the coverage of surface current monitoring off southwestern Taiwan has become more comprehensive with less blind data in certain regions due to land interference. As a result, the horizontal resolution is greatly improved (~4 km). Hourly data of surface current velocity are provided to the user in near real-time. Archived surface current field data from 2012 is available from TORI.

Table 1. Characteristics of the TOROS radar stations in terms of HFR installations.

Station	Frequency (MHz)	Bandwidth (kHz)	Effective ocean current observation range (km)	Resolution in range (km) / bearing (°)
SDGO, HOPN, LUYE, SHIA, SUHI, LIUK, DATN, TUTL, TWIN, PETI, CIHO, HOWN	4.580	−40.439	150	3.71/5
CIAO, LILY, MABT, BABY, FALA	13.45	−99.259	75	1.51/2
NAWN	24.300	−100.178	40	1.50/2

In this study we adopt a new skill score, based on the cumulative Lagrangian separation distance normalised by the associated cumulative trajectory length (Liu and Wesberg 2011), to evaluate the performance of trajectory modelling implied by TOROS surface currents. Ten GPS surface drifters, drogued at 1.5 m, were deployed at seas surrounding Taiwan during the period of November 2013 to August 2014 (Figure 2(a)). Following Liu and Weisberg (2011), an index s is defined as an average of separation distances weighted by the lengths of the observed trajectory. A skill score ss for trajectory models is thus defined based on s, assuming the value of tolerance threshold $n = 1$,

$$S = \sum_{i=1}^{N} di / \sum_{i=1}^{N} loi\ ,\ s \qquad s = \begin{cases} 1 - \dfrac{S}{n}, & S \leq n \\ 0, & S > n \end{cases} \tag{1}$$

where di is the separation distance between the modelled (HFRs) and observed (GPS drifter) endpoints of the Lagrangian trajectories at time step i after the initialisation. loi is the length of the observed trajectory, and N is the total number of time steps.

If the ss value equals to unity, it means that the simulated trajectory agrees fully with the observed drifter trajectory. Figure 2(b) shows the spatial distributions of skill scores in 12-hourly interval for 36-hour simulations

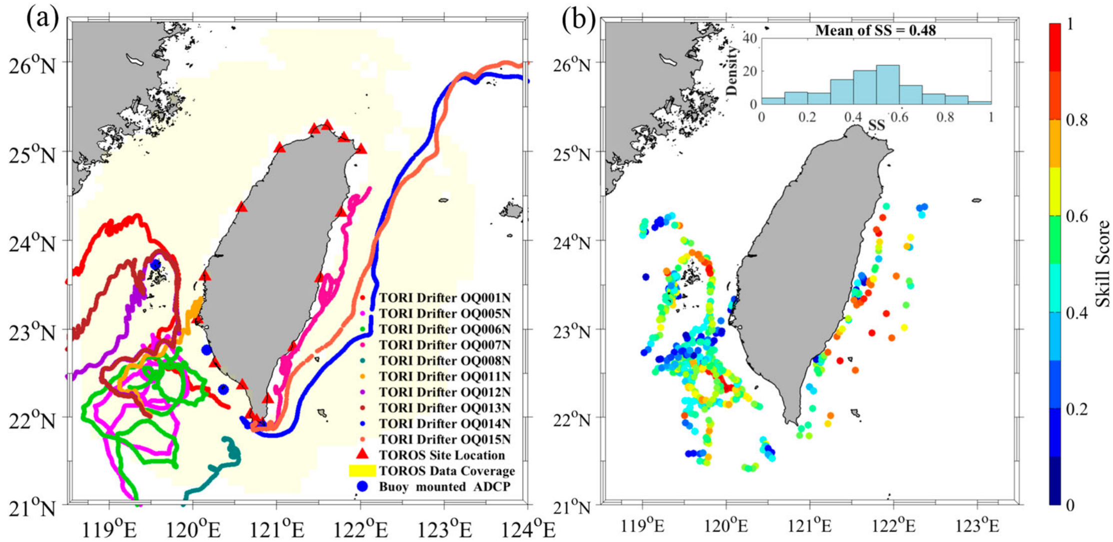

Figure 2. (a) Locations of ADCPs mounted on four data buoys (in blue solid circles) and trajectories of ten surface drifters to validate TOROS HFRs, and (b) skill scores distribution of TOROS HFRs calculated by the evaluation method proposed by Liu and Weisberg (2011) based on comparisons with ten drifters during 2013–2014.

based on the entire data set of all 10 drifters. Larger skill scores (ss = 0.3–0.7) are generally seen in the seas surrounding Taiwan. The mean ss value is 0.48. This result indicates that TOROS HFRs 10 km-grid surface currents mapping perform moderately well.

Comparison between HFR radial velocities and ADCP-derived velocities mounted on four moored data buoys off southwestern Taiwan coast was also performed (Figure 2(a)). The mean correlation coefficients and RMS differences between these two observations are 0.767 and 0.123 m/s, respectively (Table 2), again validating the performance of TOROS network.

2.2. Bottom-mounted current profilers

In addition to the ocean surface, current field data observed by the operational high-frequency coastal radars, point measurements of ocean currents can also provide useful, supplementary data for a crude estimation of drifting trajectories for missing objects. In this study, time series data of ocean current velocities collected by bottom-mounted ADCPs at two stations near the northern and southern tips of Taiwan (marked as N and S in Figure 1) were employed to understand the flow characteristics at these two sites.

Table 2. Comparison of surface velocities between data buoy-mounted ADCP and averaged HFR radials for 15 km in search radius.

Buoy	Radar site	Correlation coefficient	Root mean square difference (m/s)
Penghu Buoy	TWIN	0.781	0.136
Mituo Buoy	CIHO	0.812	0.078
Eluanbi Buoy	NAWN	0.679	0.152
Eluanbi Buoy	BABY	0.745	0.123
Xiao Liuqiu Buoy	CIHO	0.769	0.114
Xiao Liuqiu Buoy	HOWN	0.813	0.132
MEAN		0.767	0.123
MAX		0.813	0.152
MIN		0.679	0.078

The ADCPs are of the type of Nortek Aquadopp Profiler with an acoustic frequency of 1 MHz. Mounted on a steel frame, an ADCP and a Sea-Bird Electronics wave/tide gauge were deployed at seabed of about 20 m deep. The ADCP heads were situated about 0.5 m off the bottom. The bin size and sampling interval were set to be 1 m and 10 minutes, respectively. At the station N, the observed current velocity profiles from three data sets, during 2012/9/3–2012/10/21, 2012/10/22–2012/11/21, and 2013/3/8–2013/4/9, were collected. At the station S, deployment of the ADCP was conducted regularly in each season from 2013 to 2018 with the recording length for each deployment ranged between 15 days and one month.

The currents and tidal elevation data return were excellent and required minimal editing. Pitch, roll, and heading values of the ADCP were checked first to ensure that the bottom mounting frame was sitting steadily on the seabed without significant movements. Raw current velocity data was then checked for any anomalous data points. Data outliers, usually very rare, were deleted and the gap was filled by cubic splines interpolation. The recorded current velocities have an accuracy of 1% ± 0.5 cm/s.

3. Object drifting trajectory estimation

This study makes use of two approaches to estimate movements of drifting objects and missing persons at sea. The first approach is a simple estimation of particle displacement with time from its LKP driven by the background ocean surface currents derived from the nearest grid of TOROS data assuming negligible waves and wind-induced leeway effect. This method is similar to the conventional progressive vector diagram (PVD) which has been used to estimate transport in the coastal ocean from point measurements of velocity time series (Carlson et al. 2010). In this study, surface transport is estimated based on PVDs using synoptic surface currents measured by HF radar. The advantage of this method is that it provides a rapid response to deal with the SAR emergency for saving lives in cases of missing PIW.

The second approach is by use of SARMAP, a commercialised model and response system for marine SAR developed by Applied Science Associates, in conjunction with environmental input data (specifically wind and surface current) and the object's drift behaviour for rapid predictions of the movements of drifting objects and missing persons. SARMAP computes drift derived by wind leeway, leeway divergence and ocean current with two optional modules, i.e. IAMSAR and Monte Carlo methods. In this study, we adopted the Monte Carlo simulator (O'Donnell et al. 2005; Breivik and Allen 2008) with a user-specified number of imaginary particles released near the reported LKP to generate a dynamic probability density map for object drifting prediction and search planning. The Markov's Monte Carlo method takes the spatial and temporal variations of drifting objects into account, as well as the uncertainty of input environmental information and leeway parameters. The simulation results are presented in a time-varying spatial probability density map, which clearly shows the possible drift path of the target.

4. Case studies of marine SAR

In order to demonstrate the importance and necessity of ocean observations for use in marine safety, two cases of marine incidents are studied in the present study. These two cases are selected because of their different characteristics in ocean currents and marine climate, object's shape and drift behaviour. This will allow us to have a deep investigation on how the drift tracks might vary with respect to environmental input data. In each case, the predicted and actual found positions based on two methods of calculations are compared.

4.1. Case I: PIW in a tidal bay

On 8 June 2015, the TCGA command centre received a report of a missing person on the Tamsui coast, northern Taiwan. The time of the call was 2031 local time and the LKP was at 25°15′N and 121°28′E. Wearing a life jacket, this person was on a recreational boat and was thrown overboard when this boat capsized. The TCGA immediately dispatched SRUs to the site. After hours of intensive search by ships and helicopters, the missing person was still not found. Finally and luckily, this missing person was found and recovered alive by a fishing boat passing by this area at 25°16′N and 121° 27′E, about 3 km offshore of the LKP on 1600 local time of 9 June 2015.

Ocean currents at the site of the Case I are dominated by semi-diurnal tides with the M_2 tidal ellipse displaying a rectilinear shape in the NE/SW direction according to previous studies of numerical modelling (Jan et al. 2002) and shipboard ADCP observations (Wang et al. 2004). In the past few years, we have repeatedly conducted ocean current measurements by using a bottom-mounted ADCP at a nearby site (station N in Figure 1) about 8 km south of the case I, just outside of the Taipei Harbor, for the long-term monitoring and prevention of possible oil dispersal. The observed current velocities from three data sets are used in this study for SAR purposes. As shown in Figure 3(a) is the current rose diagram from these three data sets, indicating that currents flow primarily in the tidal reciprocal directions of ENE/WSW with the speed range mostly between 40–60 and 60–80 cm/s. Mean current velocity at various tidal phases is shown in Figure 3(b) from simultaneous hourly data of sea surface elevation and current velocity. Zero up-crossings were used to determine the timing when high water, the flood phase (i.e. 1–6 hours before high water), and the ebb phase (1–6 hours after high water) occur. Figure 3(b) indicates that during the flood phase (−1 to −6 hours) mean ocean currents flow southwestward with a maximum speed of about 60 cm/s. Similar results are true during the ebb phase but for northeastward currents (1–6 hours). In short, current velocity from this point measurements illustrates a symmetrical feature between the flood and ebb tidal flows. If the ocean currents data is insufficient or unavailable at the time and place of marine incident, the mean current velocities at various tidal phases derived from archived current data as shown in Figure 3(b) can be used to quickly estimate the particle drifting trajectory.

Hourly surface currents field data in 10-km horizontal resolution and wind data for the Case I is available from TOROS and Central Weather Bureau. Wind speed was generally small (lower than 5 m/s) in June. Therefore,

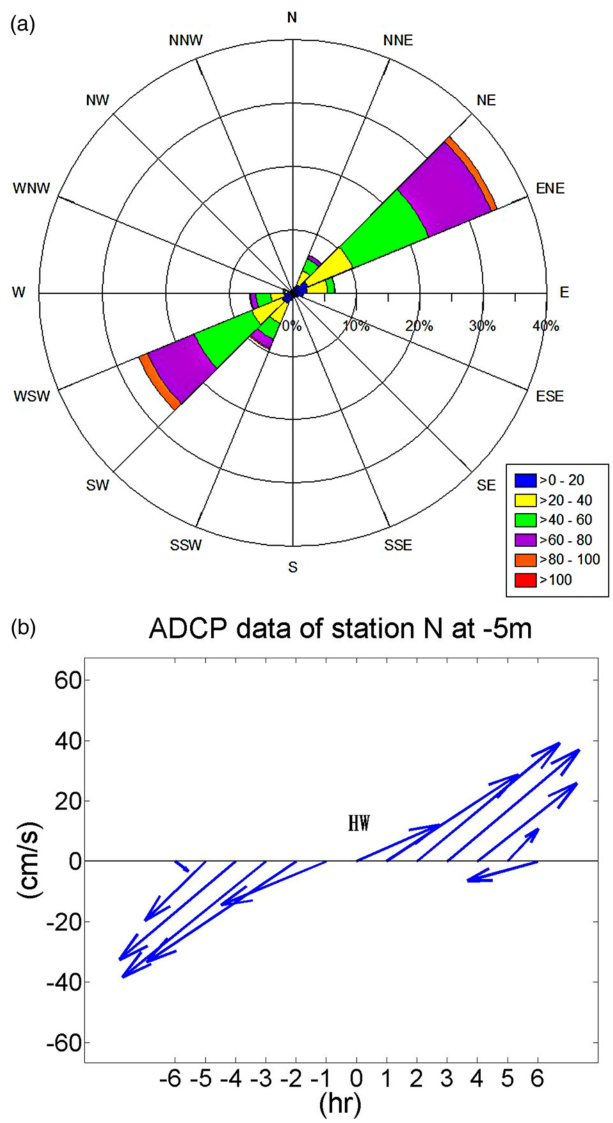

Figure 3. (a) Surface current rose diagram and (b) averaged current velocities at various tidal phases based on bottom-mounted ADCP data at station N during 2012 and 2013. HW means high water at time 0. Negative and positive time means before and after high water, respectively.

it is reasonable to neglect the wind-induced leeway effect in this case. We use two methods to estimate the particle drifting trajectory. In the first method, TOROS gridded hourly surface current data from the time of the LKP to the time of recovery was applied to evaluate the particle movements with the initial position at LKP. A simple linear scheme is adopted to calculate the distance driven by the background current in a time step of one hour. Figure 4 shows the simulated drifting trajectory of the missing person for the Case I. The simulated trajectory indicates that the person was carried by the tidal currents back and forth in the NE/SW direction. The tidal excursion was approximately 10 km, which is consistent with a rough estimate of the distance moved by a rectilinear tidal current of 0.5 m/s speed during the flood or ebb phases of 6 hours. The ending point after the 20-hour simulations turns out to be located within the same small bay, just about 3 km offshore of the LKP. The ending point and the actual recovery point are quite close, indicating that our first method is capable to generate good results.

A commercial software 'SARMAP' is used in this study as a second method to determine the object's most probable locations of detection under different types of uncertainties. Oceanic environment data (wind and current field data) and object's shape are required input for SARMAP to predict drifting object trajectory. Surface current gridded data of TOROS collected by high-frequency coastal radars are used for SARMAP calculations. Wind field reanalysis data is obtained from Weather Research and Forecasting (WRF) model provided by the Central Weather Bureau. Note that the influence of waves is not considered in this study. Wind-induced leeway speed and divergence depend on the wind speed and immersion ratio (the ratio of the part below the seawater to that of above the seawater), which varies with the shape of the object. In this case, the PIW was wearing a personal flotation device (PFD) of sitting type I or II. According to the Australian National SAR manual (2017 Edition), values of leeway speed and divergence can be determined from their table for different categories. Figure 5 shows the spatial distribution of drift probability from SARMAP output results calculated by the Monte Carlo method for 100 virtual particles released in the LKP for the Case I after the 20-hour simulations. Note that in Figure 5 the more points in a box represent the higher probabilities that the missing person can be found in that area. The actual recovery position is located at a box with the highest probabilities (Figure 5), confirming the good outcome of the SARMAP in combination with the oceanic environment data of wind and current, and the object's PFD type.

4.2. Case II: PIW in eddy-affected zone

On 18 February 2017, TCGA received a report that a fishing raft sailed out from Dapeng Bay, southwestern Taiwan early morning but did not return by 1000 local time as scheduled. There was only one fisherman onboard this raft. On 1500 of that day, the capsized raft was found near the beaches with wave breaker blocks of Dapeng Bay. The LKP was at approximately 22°27′13″N and 120°26′0″E, but the fisherman was nowhere to be found. The body of the fisherman was found five days later, on 23 February 1000 local time off the southern tip of Taiwan, about 70 km south of the LKP.

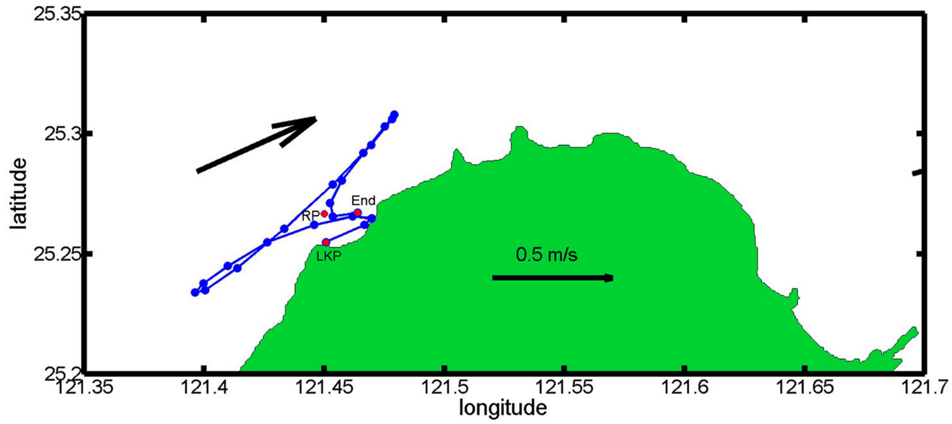

Figure 4. The object's drifting trajectory for the case I based on the simple advection driven by HFRs-derived surface currents. LKP is the last known position. END is the ending position of trajectory. RP is the actual recovery position. The black vector represents the surface current of the nearest grid.

Mesoscale eddies, mostly anticyclonic warm-cores, were often seen to exist southwest of Taiwan from multi-satellite altimetry (Cheng et al. 2014) and from 20-year model reanalysis data (Chang et al. 2015). These oceanic eddies can alter the Taiwan Strait currents and even modify the coastal flows on the shelf (Chang et al. 2015). We have conducted repeatedly measurements of ocean currents in the coastal waters off Howan, about 9 km north of Taiwan's southern tip (marked as S in Figure 1) for several years in order to make a long-term environmental evaluation and impact assessment for National Museum of Marine Biology and Aquarium. The long-term observed current velocities at the station S provide useful information of background flows for the Case II. Figure 6(a,b) shows the current rose diagram and mean current velocities at various tidal phases, respectively based on current velocities data of 2013–2018 between January and March. The current rose diagram (Figure 6(a)) manifests a fact that the currents flow primarily in SSW and the speeds range mostly between 20 and 40 cm/s. Mean current velocities at various tidal phases (Figure 6(b)) indicates that during floods (−1 to −6 hours) mean currents are weak (~5 cm/s) and flowing northward. Ebb flows (1–6 hours), on the other hand, are much stronger (5–25 cm/s) and flowing towards SSW. This feature of

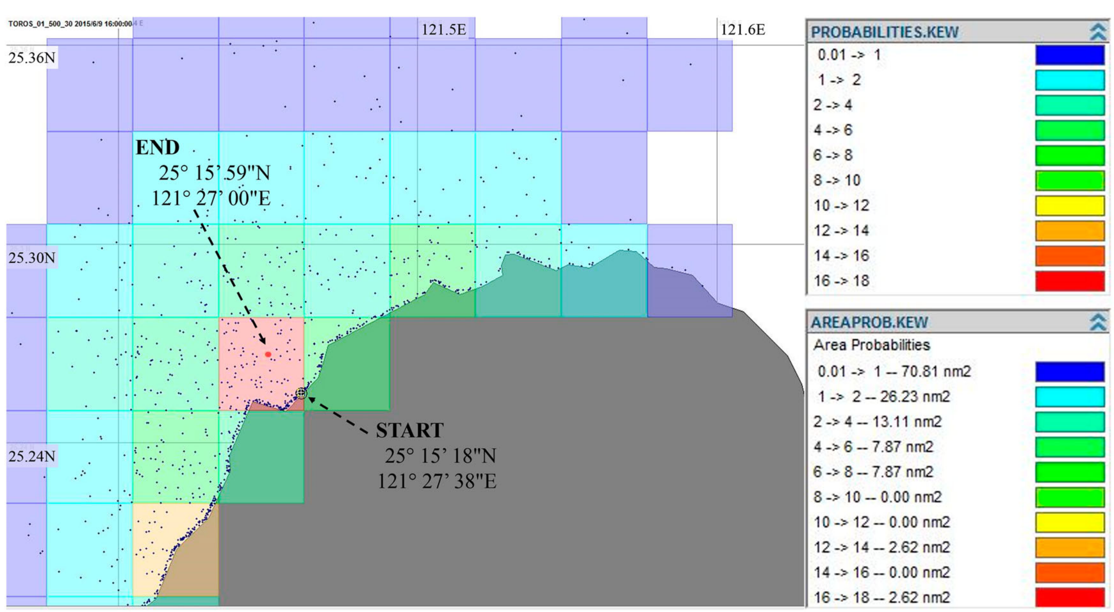

Figure 5. Distribution of ending positions from drifting simulations by the Monte Carlo based SARMAP with 1000 imaginary particles released at the location marked as 'Start' for the case I. Colours in each box denote the probabilities of detection. The most probable region to find the object is shown as the pink box. The 'End' denotes the actual recovery position.

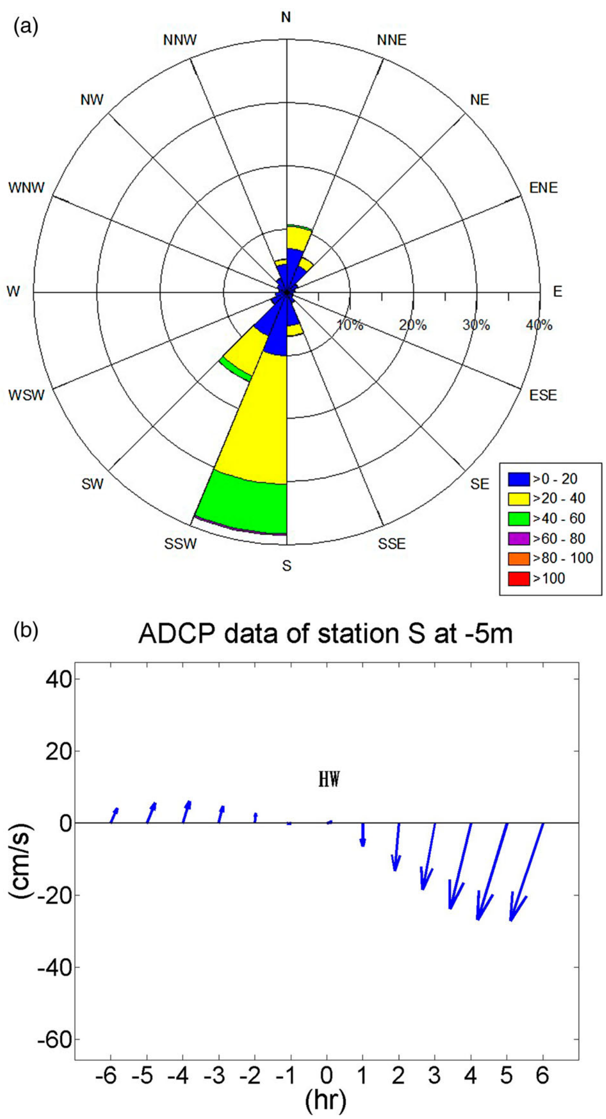

Figure 6. (a) Surface current rose diagram and (b) averaged current velocities at various tidal phases based on bottom-mounted ADCP data at station S during 2013 to 2018, January to March. HW means high water at time 0. Negative and positive time means before and after high water, respectively.

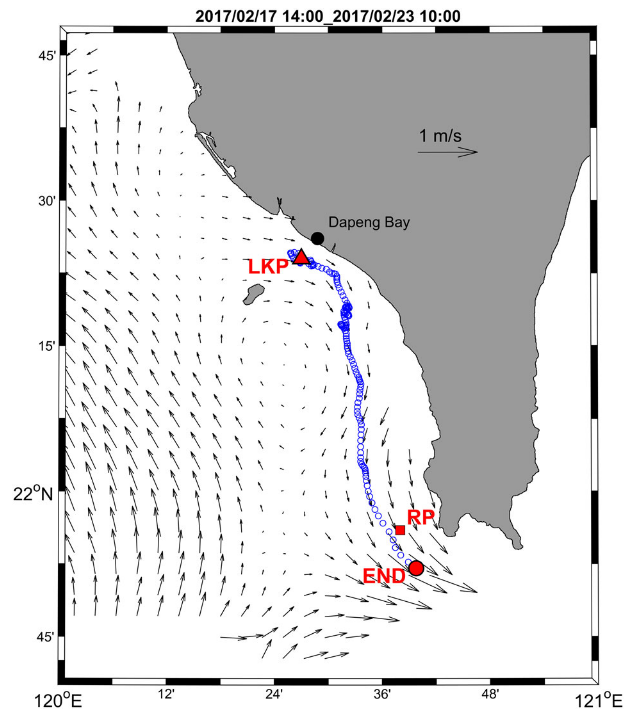

Figure 7. The object's drifting trajectory for the case II based on the simple advection driven by ocean currents. Red triangle is the starting position of simulations. Red circle is the ending position of simulations. Red square is the actual recovery position. Surface current field averaged over the simulation period is overlaid on this figure.

predominantly southward flow along the southwestern coast of Taiwan almost always occurs all year round from our long-term point measurements of currents. The mechanism of this southward flows is likely due to an anticyclonic warm eddy in this region and is a subject worthy of further pursuit.

As in Case I, TOROS gridded hourly surface current data is used in the first method to calculate the particle drifting trajectory for the case II. However, unlike case I, the LKP location and time for the case II were not certain according to TCGA's report, only the recovery point and time were known. Note that the HFRs network over the southwestern Taiwan coast has been upgraded since July 2016 by adding one extra, temporary station of FALA (Figure 1). As a result, a finer horizontal resolution (~4 km) of the TUV data in this region was attained, in comparison with the previous resolution of 10 km. Figure 7 shows the simulated drifting trajectory of the missing fisherman for a time span of 120 hours overlaid with the averaged current field, assuming a reasonable LKP time and location. From TOROS-derived current field, a persistent southward flow is seen to exist along the coast, which is separated from the northward current in deeper waters offshore by a band of calm waters in between. The body was carried by the coastal flow towards the south, travelling a distance of about 70 km to near the southern tip of Taiwan where the body was finally found five days later. This travelled distance and the time spent correspond to a mean southward current speed of 0.15–0.2 m/s which is consistent with the observed currents at the station S.

SARMAP is also utilised in this case to estimate the object's most probable locations of detection based on the TOROS current field data and WRF wind field reanalysis data, assuming the PIW was not wearing a PFD. The spatial distribution of drift probabilities from 1000 virtual particles released in the LKP for the Case II after 120-hour simulations is shown in Figure 8. At the end

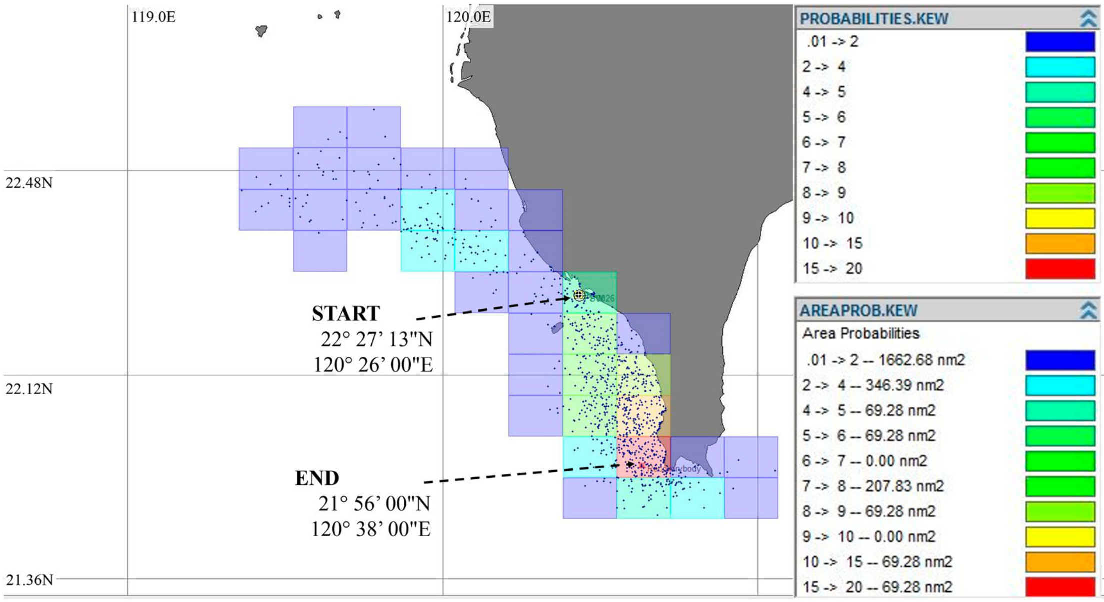

Figure 8. Distribution of ending positions from drifting simulations by the Monte Carlo based SARMAP with 1000 imaginary particles released at the location marked as 'Start' for the case II. Colours in each box denote the probability of finding the object. The most probable region to find the object is shown as the pink box. The 'End' denotes the actual recovery position.

of simulations, all 1000 particles were spreading in a wide area, some were located at the north of LKP, but more were distributed along the coastal region toward the south of LKP. The box with the most number of particles was located near the southern tip of Taiwan, which is in agreement with the actual recovery position. This box represents the most probable area to find the PIW, and SRUs should be sent with high priority to this area.

5. Discussion

5.1. Importance of HFRs and supplemental ocean observations

Two different datasets of ocean surface currents from TOROS were used in simulations of case II off southwestern Taiwan, that is, the dataset with regular resolution of 10 km and the dataset with finer resolution of 4 km. As mentioned earlier, for the coverage area off southwestern Taiwan a finer resolution of 4 km can be achieved by adding one extra, temporary radar station in FALA (Figure 1). Simulation results based on the finer resolution dataset (Figures 7 and 8) reveal southward particle drift trajectories which are generally consistent with the actual reality for this case. On the other hand, if the ocean current dataset with 10 km is used, the simulation results show the northward particle drift trajectory (figure not shown). In other words, TOROS surface currents with 10 km resolution cannot fully disclose detailed flow patterns, particularly along the southwestern coast of Taiwan, that has a big impact on the prediction of particles drift trajectory for the case II. This leads to an important conclusion that accurate and comprehensive observations of ocean current mapping by HFRs are one of the most essential elements for the societal needs of marine safety.

Point measurements of ocean current by ADCPs or current metres provide another useful means to supplement HFRs current mapping and sometimes can also be used for a first-step crude estimate of particles drifting in SAR missions. These observations are mostly research-oriented, so the instrumentation, location, and data specifications vary. Nevertheless, the collection of these observed data on a long-term basis are very important tasks. Applications of the statistics of ocean currents including the most frequently occurred current speed and direction in weak-tide but eddy-affected region (case II) and the averaged tidal currents oscillations at various tidal phases in the strong-tide region (case I) prove to be very useful for rapid response of marine incidents.

5.2. Real-time data and forecast of ocean currents

Case studies in this study are applications of hindcast of ocean currents. In the event of marine incidents with the need of rapid response for SRUs dispatch, real-time observed data and forecast of wind, waves, and currents from a few hours up to a few days ahead are the requirement for the prediction of object's drift trajectory. HFRs current field data of TOROS routinely operated by TORI is transmitted to TCGA and CWB in near real-time mode as the oceanic environment input data to drive SARMAP or SAROPS in cases of marine incidents. CWB also routinely operates some 18 data buoys in coastal waters surrounding Taiwan, constantly observing marine meteorology and sea state (wind, waves, temperature, sea-level pressure); among them 13 buoys also measure current profiles. For prediction purposes, the forecast of ocean data from operational ocean models such as the POM T3/N2 model of TORI, the OCM2-NEW model of CWB is available in the regional domain surrounding Taiwan. These in-situ observations of ocean currents in near real-time and the forecast of ocean currents from models are important for societal needs for marine safety and other applications.

6. Concluding remarks

Two cases of marine incidents of PIW were analysed with different ocean current characteristics; strong semi-diurnal tides in the case I versus weak tide but with predominantly southward flow affected by eddies in the case II. By incorporating surface current field data provided by the operational HFRs supplemented by wind data, a Monte Carlo, random walk based system of SARMAP was employed to these two cases with consistent results obtained between simulated and actual recovery locations. On the other hand, point measurements of ocean currents by using two bottom-mounted ADCPs with limited recording lengths (a few months to a few years), still prove to be useful for a crude estimate of the fate for the drifting of missing PIW in these two cases. Comparisons between radar-derived flow fields from regular and intensified HFRs system in southwestern Taiwan indicates that the latter has better abilities to resolve detailed flow structures, particularly along the coast. This difference in flow-resolving will result in poor and inconsistent simulation consequences based on the current field data derived from the former HFRs. In conclusions, we have demonstrated through two case studies that operational ocean observations by HFRs are extremely useful for marine SAR. Even the short-period point measurements of ocean currents, if used properly, can benefit the use of marine safety.

Acknowledgments

Taiwan Ocean Research Institute (TORI) operates the 18-HFRs system. Information about the time and locations for the two cases of marine incidents is provided by TCGA. Wind reanalysis data and buoy-mounted ADCP data are provided by Taiwan CWB.

Disclosure statement

No potential conflict of interest was reported by the authors.

Funding

This research was completed with grants from Ministry of Science and Technology Taiwan (MOST 106-2611-M-110-003).

References

Breivik O, Allen AA. 2008. An operational search and rescue model for the Norwegian Sea and the North Sea. J Mar Sys. 69(1/2):15.
Breivik O, Allen AA, Maisondieu C, Olagnon M. 2013. Advances in search and rescue at sea. Ocean Dyn. 63:83–88.
Carlson DF, Muscarella PA, Gildor H, Lipphardt BL, Jr., Fredj E. 2010. How useful are progressive vector diagrams for studying coastal ocean transport. Limnol Oceanogr Method. 8:98–106.
Chang YL, Miyazawa Y, Guo X. 2015. Effect of mesoscale eddies on the Taiwan strait current. J Phys Oceanogr. 45:1651–1666.
Cheng YH, Ho CR, Zheng Q, Kuo NJ. 2014. Statistical characteristics of mesoscale Eddies in the North Pacific derived from satellite altimetry. Remote Sens. 6:5164–5183.
Crombie DD. 1955. Doppler spectrum of sea echo at 13.56 mc/s. Nature. 175:681–682.
Falco P, Buonocore B, Cianelli D, De Luca L, Giordano A, Iermano I, Kalampokis A, Saviano S, Uttieri M, Zambardino G, Zambianchi E. 2016. Dynamics and sea state in the Gulf of Naples: potential use of high-frequency radar data in an operational oceanographic context. J Operation Oceanogr. 9(supp1):s33–s45.
Harlan J, Terrill E, Hazard L, Keen C, Barrick D, Whelan C, Howden S, Kohut J. 2010. The integrated ocean observing system high-frequency radar network: status and local, regional, and national applications. Mar Technol Soc J. 44:122–132.
Jan S, Wang J, Chern CS, Chao SY. 2002. Seasonal variation of the circulation in the Taiwan Strait. J Marine Sys. 35:249–268.
Liu Y, Weisberg RH. 2011. Evaluation of trajectory modeling in different dynamic regions using normalized cumulative Lagrangian separation. J Geophys Res. 116(C09013). doi:10.1029/2010JC006837.
O'Donnell J, Ullman D, Spaulding M, Howlett E, Fake T, Hall P, Tatsu I, Edwards C, Anderson E, McClay T, Kohut J, Allen A, Lester S, Lewandowski M. 2005. Integration of Coastal Ocean Dynamics Application Radar (CODAR) and Short-Term Prediction System (STPS) surface current estimates into the search and rescue Optimal Planning System (SAROPS). US Coast Guard Technical Report, CG-D-01-2006.
Ohlmann JC, White PF, Sybrandy AL, Niiler PP. 2005. GPS–cellular drifter technology for coastal ocean observing systems. J Atmos Ocean Technol. 22:1381–1388.
Ohlmann JC, White PF, Washburn L, Terrill E, Emery B, Otero M. 2007. Interpretation of coastal HF radar–derived

surface currents with high-resolution drifter data. J Atmos Oceanic Technol. 24:666–680.
Paduan JD, Washburn L. 2013. Observation of ocean surface currents. Annu Rev Mar Sci. 5:115–136.
Wang YH, Jan S, Wang DP. 2004. Transports and tidal current estimates in the Taiwan Strait from shipboard ADCP observations (1999–2001). Estuarine Coastal Shelf Sci. 57:193–199.
Yao CT, Tsai CH, Hsu HH. 2016. Applications of datum marker buoy data to search and rescue of persons in water. J Mar Sci Technol. 24:631–636.
Zhang J, Teixeira AP, Soares CG, Yan X. 2017. Probabilistic modelling of the drifting trajectory of an object under the effect of wind and current for maritime search and rescue. Ocean Eng. 129:254–264.